Report

Cell Reports

Positioning of AMPA Receptor-Containing Endosomes Regulates Synapse Architecture

Graphical Abstract

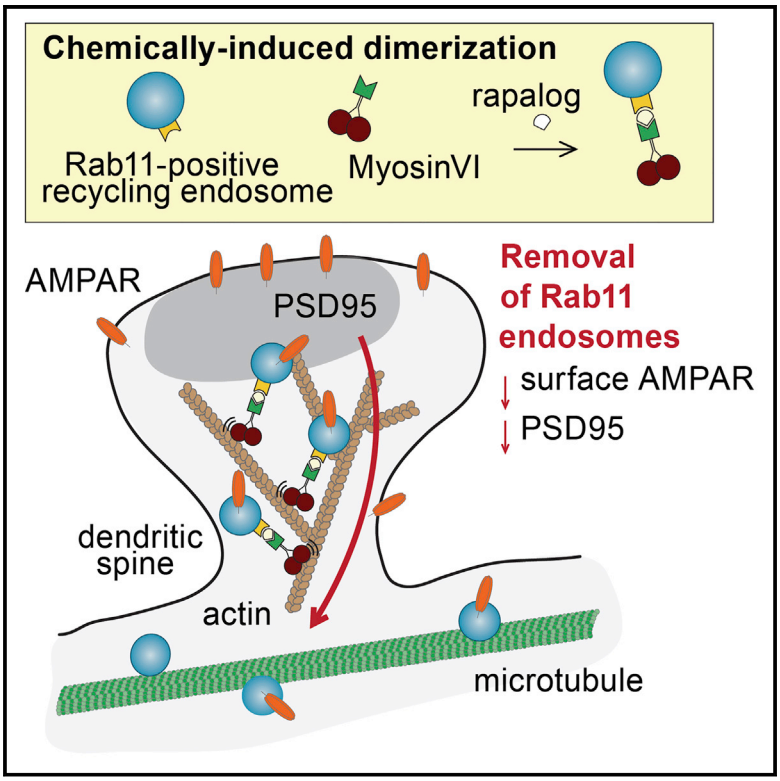

Authors

Marta Esteves da Silva, Max Adrian, Philipp Schätzle, ..., Corette J. Wierenga, Lukas C. Kapitein, Casper C. Hoogenraad

Correspondence

l.kapitein@uu.nl (L.C.K.), c.hoogenraad@uu.nl (C.C.H.)

In Brief

In this study, Esteves da Silva et al. report an approach to temporally control endosomal trafficking in dendritic spines. Induced removal of recycling endosomes decreases surface AMPA receptor expression and PSD-95 clusters at synapses, suggesting that endosome positioning is an important factor in controlling synapse architecture.

Highlights

- Visualization of AMPA receptors trafficking in recycling endosomes in dendrites
- Trafficking of Rab11 endosomes depends on both microtubule and actin cytoskeleton
- Effective temporal control of endosomal trafficking in dendritic spines
- Induced removal of recycling endosomes from spines affects synapse architecture

Esteves da Silva et al., 2015, Cell Reports *13*, 933–943
November 3, 2015 ©2015 The Authors
http://dx.doi.org/10.1016/j.celrep.2015.09.062

Cell Reports
Report

Positioning of AMPA Receptor-Containing Endosomes Regulates Synapse Architecture

Marta Esteves da Silva,[1] Max Adrian,[1] Philipp Schätzle,[1] Joanna Lipka,[1,3] Takuya Watanabe,[4] Sukhee Cho,[4] Kensuke Futai,[4] Corette J. Wierenga,[1] Lukas C. Kapitein,[1,2,*] and Casper C. Hoogenraad[1,2,*]
[1]Cell Biology, Faculty of Science, Utrecht University, 3584 CH Utrecht, the Netherlands
[2]Department of Neuroscience, Erasmus Medical Center, 3015 GE Rotterdam, the Netherlands
[3]International Institute of Molecular and Cell Biology, 02-109 Warsaw, Poland
[4]Department of Psychiatry, Brudnick Neuropsychiatric Research Institute, University of Massachusetts Medical School, Worcester, MA 01605, USA
*Correspondence: l.kapitein@uu.nl (L.C.K.), c.hoogenraad@uu.nl (C.C.H.)
http://dx.doi.org/10.1016/j.celrep.2015.09.062

SUMMARY

Lateral diffusion in the membrane and endosomal trafficking both contribute to the addition and removal of AMPA receptors (AMPARs) at postsynaptic sites. However, the spatial coordination between these mechanisms has remained unclear, because little is known about the dynamics of AMPAR-containing endosomes. In addition, how the positioning of AMPAR-containing endosomes affects synapse organization and functioning has never been directly explored. Here, we used live-cell imaging in hippocampal neuron cultures to show that intracellular AMPARs are transported in Rab11-positive recycling endosomes, which frequently enter dendritic spines and depend on the microtubule and actin cytoskeleton. By using chemically induced dimerization systems to recruit kinesin (KIF1C) or myosin (MyosinV/VI) motors to Rab11-positive recycling endosomes, we controlled their trafficking and found that induced removal of recycling endosomes from spines decreases surface AMPAR expression and PSD-95 clusters at synapses. Our data suggest a mechanistic link between endosome positioning and postsynaptic structure and composition.

INTRODUCTION

Most fast excitatory signaling in the brain is mediated by AMPA-type glutamate receptors, and changes in the number of these receptors at synapses are thought to underlie information storage in the brain (Huganir and Nicoll, 2013). AMPA receptors (AMPARs) exchange between synaptic and extrasynaptic sites by lateral diffusion in the plasma membrane, whereas endosomal recycling and trafficking followed by exocytosis is believed to maintain a supply of extrasynaptic AMPARs on the membrane (Czöndör et al., 2012; Newpher and Ehlers, 2008). However, the spatial coordination between these two major AMPAR transport mechanisms has remained unclear, because, in contrast to lateral receptor diffusion, little is known about the dynamics of AMPAR-containing endosomes.

Excitatory synapses are located mostly at small dendritic protrusions, called spines, which are often connected to the dendritic shaft through a narrow membrane tube of 100–200 nm diameter, called the spine neck. This architecture is believed to biochemically isolate the spine from the rest of dendrite, because it slows down both cytoplasmic and membrane-based diffusion. Simulations have suggested that secretion inside spines dramatically increases the fraction of receptors captured at synapses, compared to secretion near the base of the spine neck (Adrian et al., 2014). In addition, endosomes are known to often function as a signaling hub, and their precise position either inside or outside spines would strongly affect signaling persistence, given the biochemical isolation of spines (Colgan and Yasuda, 2014). However, how the positioning of AMPAR-containing endosomes affects synapse architecture has never been directly explored.

Here we use high-resolution live-cell imaging to examine the intracellular dynamics of AMPAR-containing endosomes. We found that AMPARs move in highly dynamic Rab11 endosomes that frequently enter and exit dendritic spines. Whereas long-range transport is largely microtubule (MT)-based, spine entries mostly depend on actin-based myosin motors. By repositioning endosomes, we found that removal of recycling endosomes from dendritic spines decreased the level of AMPAR at the spine membrane, as well as PSD-95 clusters at synapses. Our data demonstrate that recycling endosome trafficking directly affects synaptic function, and they suggest a mechanistic link between endocytic recycling and the structure and composition of the synapse.

RESULTS

Intracellular AMPARs Are Transported in Recycling Endosomes

To directly probe AMPAR vesicle trafficking in hippocampal neurons, we co-expressed HA-GluA1 and GFP-GluA2 and precisely controlled the timing and level of GFP-GluA2 receptor expression using a doxycycline (DOX)-regulated gene expression

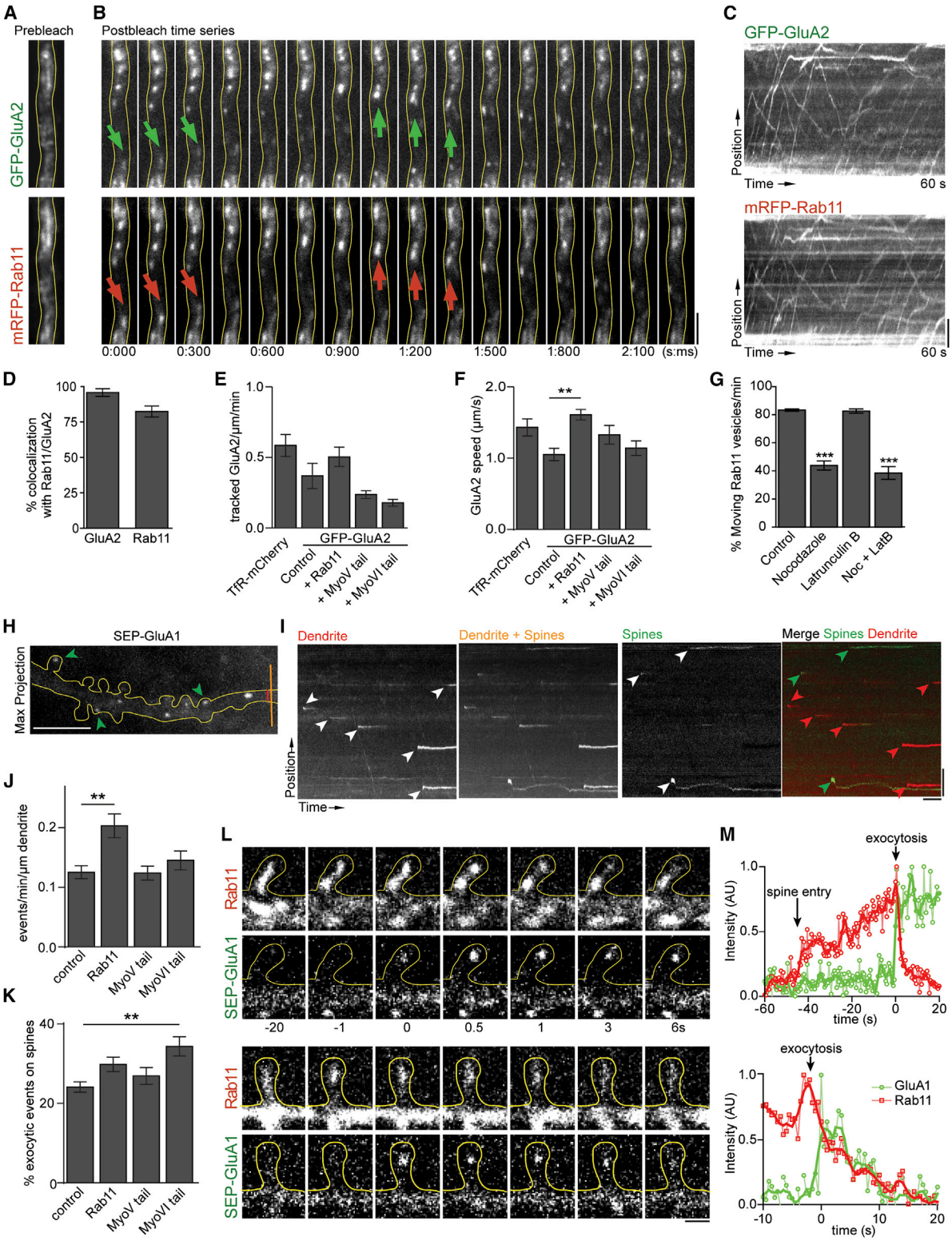

Figure 1. Rab11-Positive Recycling Endosomes Transport GluA1/A2 in Dendrites and Spines

(A and B) Stills from a dual-color time-lapse recording of a rat hippocampal neuron expressing GluA1, GFP-GluA2 (top), and mRFP-Rab11 (bottom). (A) Pre-bleach overview of GFP-GluA2 and mRFP-Rab11 and (B) post-bleach time series are shown. Arrows mark motile vesicles positive for both GFP-GluA2 and mRFP-Rab11.

(legend continued on next page)

system. The majority of the GluA2 receptors was localized to the plasma membrane or retained in the ER, which appeared as diffusive signals throughout the dendrites (Figure 1A). To selectively visualize intracellular vesicular GFP-GluA2, most of the fluorescence from the dendritic part in the field of view was bleached before image acquisition. Neurons expressing low levels of GFP-GluA2 revealed vesicle-like structures in the dendritic shaft and dendritic spines that were moving rapidly (Figures 1A and 1B). In the dendritic shaft, GFP-GluA2 motility was directed both away from and toward the cell body and reversals also frequently were observed (Figure 1C). Intracellular AMPARs most likely follow the endosomal transport routes (Brown et al., 2007; Hoogenraad et al., 2010; Park et al., 2004, 2006; Wang et al., 2008).

To examine the identity of GFP-GluA2-containing vesicles, neurons were co-transfected with HA-GluA1 and GFP-GluA2 and stained for Rab11, a marker for recycling endosomes. Due to the high abundance of GluA1/2 in other cellular compartments, only a minor fraction was colocalized with endogenous Rab11 in fixed neurons (Figures S1A and S1B). Live-cell imaging in conditioned medium with constant osmolality showed that ~80% of Rab11-positive recycling endosomes in the dendrites are motile (Figures S2A–S2E). Live imaging directly after bleaching revealed that 96.0% ± 1.5% of the motile GFP-GluA2-containing vesicles contained mRFP-Rab11, whereas 77.6% ± 1.2% of all motile Rab11-positive vesicles also contained GluA2 (Figure 1D; Table S1). The average density of moving GFP-GluA2 vesicles was 0.37 ± 0.09 μm/min (Figure 1E), with a mean vesicle velocity of 1.05 ± 0.09 μm/s in control conditions (Figure 1F). Co-expression of Rab11 increased the GluA2 vesicle speed to values similar to those for endosomal vesicles with Transferrin Receptor (TfR) (Figure 1F). Interestingly, highly dynamic clusters of GluA2 could be observed within the motile Rab11-positive recycling endosomes (Figures S1C–S1I). These intra-endosomal subdomains may localize signal responses or concentrate components for further endosomal sorting.

We next determined whether Rab11 vesicle trafficking in dendrites depends on the actin or MT cytoskeleton. While blocking F-actin assembly by latrunculin B (10 μM) treatments did not affect Rab11 vesicle dynamics along the dendrites, the addition of low concentrations of nocodazole (300 nM) to inhibit MT dynamics decreased their motility to ~40% (Figures 1G, S2F, and S2G). After nocodazole treatment, the majority of the Rab11-positive recycling endosomes accumulated in enlarged and immobile clusters in the dendritic shaft. The addition of nocodazole and latrunculin B to the neurons had a similar effect as nocodazole alone (Figures 1G, S2F, and S2G). Consistently, expression of dominant-negative constructs to abrogate MyosinV or MyosinVI function did not affect the GFP-GluA2 vesicle speed (Figure 1F). These results suggest that intracellular AMPARs are transported in Rab11-positive recycling endosomes along dynamic MT tracks within the dendritic shaft.

Endosomal Entry in Spines Correlates with an Increase in Surface AMPARs

SEP-labeled GluA subunits have been used to visualize postsynaptic exocytosis in dendrites and AMPAR dynamics on the plasma membrane. Here we determined the correlation between recycling endosome dynamics and AMPAR exocytosis by simultaneously imaging tagRFP-Rab11 and SEP-GluA1. As reported previously (Petrini et al., 2009), AMPARs undergo exocytosis not only in dendritic shafts but also in dendritic spines (Figure 1I). Under basal conditions, generally few exocytic events releasing GluA1 could be observed (0.13 ± 0.01 events/min/μm dendrite) (Figure 1J), but the number of events in spines contributed to 24.1% ± 1.3% of the total amount of events recorded on dendrites (Figure 1K). Co-expression of Rab11 led to a slight increase in the total number exocytic GluA1 events (Figure 1J). Some of the events in spines followed the entry of dynamic Rab11 vesicles, and the appearance of SEP-GluA1 was accompanied by the disappearance of the Rab11 signal (Figures 1L and 1M; Movie S1), suggesting a correlation between Rab11-positive recycling endosome trafficking and AMPAR exocytosis in spines. Expression of dominant-negative constructs to abrogate MyosinV or MyosinVI function did not affect GluA1 exocytosis in dendrites (Figure 1J). However, inhibiting MyosinVI increased the number of exocytic events in spines (Figure 1K). After exocytosis the SEP-GluA1 fluorescence showed two distinct behaviors in individual spines; it either remained in the spine head for prolonged times on the order of tens of seconds (Figure 1L, top) or faded within a few seconds (Figure 1L, bottom), most likely reflecting the differential GluA1 retention in

(C) Kymograph of the recording in (B) shows prevalent co-motility of GFP-GluA2 and mRFP-Rab11.
(D) Average colocalization between intracellular GFP-GluA2 and mRFP-Rab11 in dendrites is shown.
(E and F) Quantifications of the (E) number of tracked vesicles/μm/min and (F) vesicle speeds of neurons expressing TfR-mCherry or GFP-GluA2, under the indicated conditions, are shown.
(G) Quantification of the percentage of motile Rab11-positive recycling endosomes in 1-min time-lapse acquisition, under the indicated conditions, is shown.
(H and I) Quantification of SEP-GluA1 exocytic events in dendrites. (H) Maximum projection of SEP-GluA1 signal of 500 frames was recorded at 5 frames/s after bleaching the dendrite. Yellow and red bars show projection width of kymographs shown in (I). Green arrows show exocytic events in spines detected by the kymograph in (I). (I) Kymographs show dendrite in (H) with different widths to visualize exocytosis in the dendritic shaft and spines. Scale bars, 10 s and 5 μm.
(J and K) Quantifications of the number of exocytic events per dendrite (J) and the fraction of events in dendritic spines (K), under the indicated conditions, are shown.
(L) Stills from two time-lapse recordings of neurons expressing tagRFP-Rab11 (top) and SEP-GluA1 (bottom). Time is indicated relative to exocytic event in SEP channel. Solid line indicates outline of a single dendritic spine.
(M) Quantification of fluorescence intensity of tagRFP-Rab11 (red) and SEP-GluA1 (green) in dendritic spines shown in (L). Dots indicate measurements connected with dim lines, thick lines are smoothed values over four adjacent values. Upper graph reveals prolonged retention of SEP-GluA1 fluorescence in the spine head, while lower graph shows rapid loss of SEP-GluA1 signal.
Graphs represent mean ± SEM. Statistical significance was determined using the Kruskal-Wallis test or one-way ANOVA and Dunnett's multiple comparison post hoc test, respectively (**$p < 0.01$ and ***$p < 0.001$). Scale bar, 5 μm (B, C, and I). See also Figures S1 and S2 and Table S1.

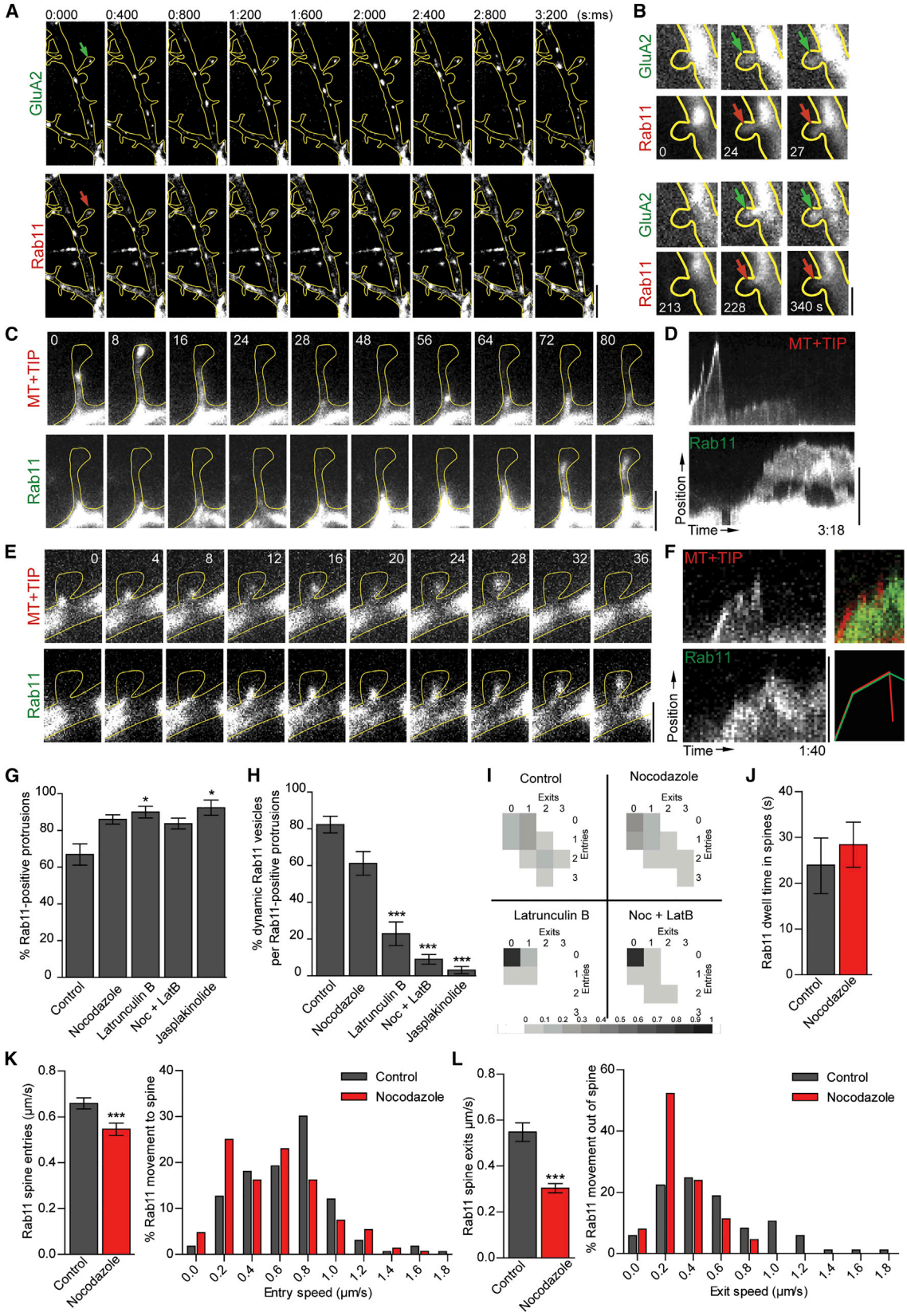

(legend on next page)

spine heads (Petrini et al., 2009). Consistently, these data suggest that recycling endosomes in spines contribute to an increase in surface AMPARs.

Recycling Endosomes Move along Both Actin and MTs in Dendritic Spines

We frequently observed Rab11 vesicles containing GFP-GluA2 in dendritic spines (Figure 2A; Movie S2). Under basal conditions, GFP-GluA2-positive Rab11 vesicles moved in and out of spines (Figures 2B and S2A). The recycling endosomes that entered spines did not necessarily emerge from immobile storage sites near the spine base, but frequently moved from distant dendritic regions. Similarly, GluA1/2-positive endosomal vesicles that left the spines were often not retained near the base of spine, but quickly moved away in the anterograde or retrograde direction within the adjacent dendrite. On average, 22.6% ± 2.3% of all immobile Rab11 vesicles were at the base of the spine (Figure S2D). To determine the role of MT and actin dynamics on Rab11-positive recycling endosome trafficking in dendritic spines, neurons were treated with low concentrations of nocodazole (300 nM) and/or latrunculin B (10 μM). In untreated live neurons at 14 days in vitro (DIV), ~65% of dendritic spines were targeted by Rab11-positive recycling endosomes, and ~80% of the endosomes in spines were dynamic (Figures 2G–2I and S3A). Nocodazole and/or latrunculin B treatment increased the number of targeted spines (Figure 2G) and decreased the endosome dynamics in spines (Figure 2H). The effect on recycling endosomal dynamics was mild in the case of nocodazole, but much more severe with latrunculin B and the combination of both drugs (Figures 2G–2I and S3A). Consistent with previous data (Correia et al., 2008; Wagner et al., 2011; Wang et al., 2008), we found that MyosinV was involved in proper endosome trafficking in spines (Figures S3B–S3E). The data also suggest that MyosinVI has a role in Rab11 vesicle transport in spines (Figure S3D). Previous studies have shown that MyosinVI is enriched in the postsynaptic density and disruption of its function leads to synaptic loss (Nash et al., 2010; Osterweil et al., 2005).

Since recent work demonstrated that spines contain dynamic MTs (Gu et al., 2008; Hu et al., 2008; Jaworski et al., 2009), we next investigated in more detail the role of MT on Rab11 vesicle dynamics in spines. To visualize MT dynamics in spines, we expressed mCherry-MT+TIP to specifically label growing MT plus ends (Yau et al., 2014). MT spine entry events were detected readily from comet displacements, and depolymerizing MTs (lacking a clear comet at the tip) also could be observed within spines (Figures 2C–2F). Co-expression of mCherry-MT+TIP and GFP-Rab11 revealed that recycling endosomes move in and out of spines in both the presence and absence of MTs (Figures 2C–2F). In untreated neurons, fast imaging of Rab11 vesicle dynamics within spines revealed that the mean entry speed was 0.66 ± 0.024 μm/s, the mean exit speed was 0.55 ± 0.04 μm/s, and the average dwell time of dynamic Rab11 vesicles was 24 s (Figures 2J–2L). Treating neurons with low concentrations of nocodazole (300 nM) decreased both the average entry and exit speeds of endosomes in spines (Figures 2K and 2L). Interestingly, inhibiting MT dynamics resulted in a marked shift of the velocity distribution profiles toward lower speeds (Figures 2K and 2L), suggesting that the velocity of Rab11 vesicles in spines is higher with MTs compared to spines without MTs. This is consistent with MT-based motility being generally faster than actin-based motility (Kapitein et al., 2013). At one point, the endosomal spine entry precisely coincided with the entry of an MT, suggesting that here Rab11 trafficking was limited by the MT growth speed (Figures 2E and 2F, entry speeds ~0.05 μm/s). Although we cannot exclude that drug treatments have an indirect effect on the Rab11 vesicle dynamics in spines, it seems likely that recycling endosomes can exploit both dynamic actin and MT-based strategies to enter dendritic spines.

Controlled Transport of Rab11-Positive Recycling Endosomes in Dendritic Spines

Translocation of Rab11-positive recycling endosomes to spines has been shown to be important for spine growth (Hoogenraad et al., 2010; Park et al., 2006). To determine the role of recycling endosomes for overall spine morphology and postsynaptic organization, we co-transfected neurons with GFP to highlight neuronal morphology and a Rab11 dominant-negative construct (Rab11-S25N) or Rab11a small hairpin RNA (shRNA). While expression of wild-type GFP-Rab11 did not affect spine morphology, blocking or depleting Rab11 highly affected the morphology of spines, showing a marked decrease in the total number of protrusions and dendritic spines (Figure 3A). To determine if the morphological effect upon disruption of Rab11

Figure 2. Recycling Endosome Transport into Dendritic Spines Depends Actin and on MT Dynamics

(A and B) Stills from a dual-color time-lapse recording of a rat hippocampal neuron expressing GluA1, GFP-GluA2 (top), and mRFP-Rab11 (bottom). Arrows mark motile vesicles positive for both markers.

(C–F) Stills (C and E) and kymograph (D and F) from a dual-color time-lapse recording of a neuron expressing GFP-Rab11 (bottom) and mCherry-MT+TIP (top). (F) Overlay of green and red channels shows complete overlap.

(G) Quantification shows the percentage of dendritic protrusions targeted by Rab11-positive recycling endosomes along 20-μm dendrite during 5-min time lapse, under different conditions.

(H) Quantification shows the percentage of dynamic Rab11-positive recycling endosomes, i.e., either one exit or one entry from a dendritic protrusion, per number of targeted protrusions, under different conditions.

(I) Schematic heatmap shows the dynamic distribution of Rab11-positive recycling endosomes in dendritic spines during 5-min time lapse, under different conditions.

(J) Quantification of Rab11 vesicles' dwell time in spines before and after nocodazole treatment is shown.

(K and L) Quantifications of Rab11-positive recycling endosomes' (K) entry and (L) exit speeds in spines, in control and nocodazole conditions, are shown.

Graphs represent mean ± SEM. Statistical significance was determined using Kruskal-Wallis test and Dunn's multiple comparison post hoc test (*$p < 0.05$ and ***$p < 0.001$; G and H) and unpaired t test with Mann-Whitney correction (***$p < 0.001$; J–L). Scale bars, 5 μm (A), 1 μm (B), and 2 μm (C–F). See also Figure S3 and Table S1.

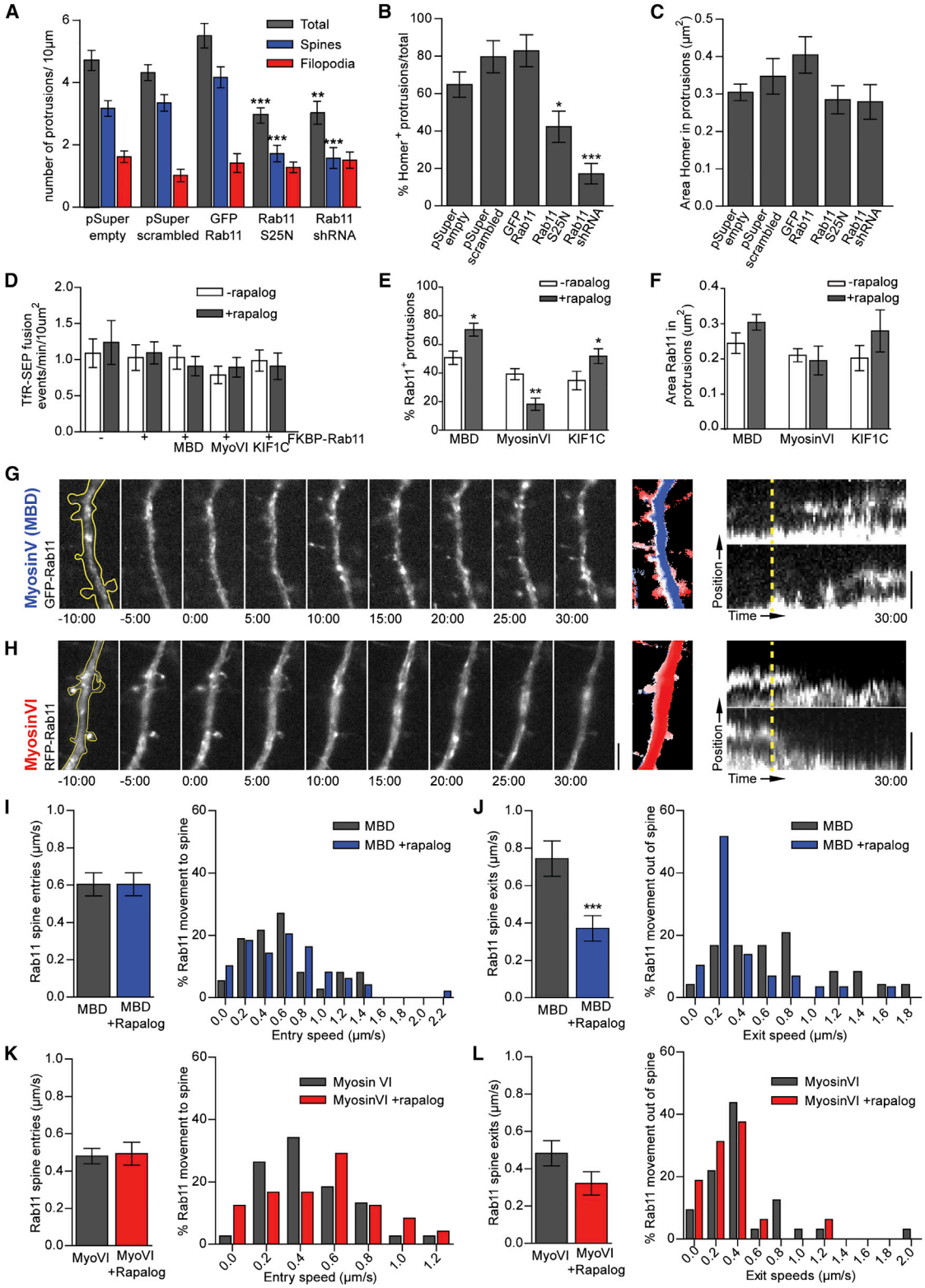

Figure 3. Time-Dependent Effect of Recycling Endosome Removal from Spines

(A) Quantification of protrusions per 10-µm dendrite. Classification was based on head width/length ratio (<0.5, filopodia; ≥0.5, spine).

(B and C) Quantifications of (B) Homer-positive protrusions per 10-µm regions of dendrite and (C) area of Homer clusters are shown.

(legend continued on next page)

correlates with changes in postsynaptic organization, alterations in the number and area of clusters of the postsynaptic marker Homer-1 were analyzed. The number of Homer-1 clusters in protrusions decreased in both Rab11 knockdown or dominant-negative conditions (Figure 3B), without significantly affecting the area of the clusters (Figure 3C). Together, these data indicate that Rab11-positive recycling endosomes play an important role in dendritic spine morphology and postsynaptic organization.

To determine the short-term effects of Rab11-positive recycling endosomes trafficking on spine morphology and synaptic function, we developed an inducible trafficking assay to directly control endosomal transport in dendritic spines. In this assay, FRB-FKBP heterodimerization was used to induce the binding of kinesin motors, myosin motors, or adaptors to Rab11 vesicles during live-cell recordings (Kapitein et al., 2010). For these experiments, Rab11 vesicles were labeled by expressing FKBP-Rab11, a fusion construct of Rab11 with FKBP12, a domain that binds to an FRB domain in the presence of rapalog AP21967 (Figure 3D). FKBP-Rab11 targeted specifically recycling endosomes (Figure S1J). FRB was fused to truncated Kinesin-3 motor KIF1C and MyosinVI motors, which contain the motor domain and coiled-coil dimerization region (KIF1C-FRB and MyosinVI-FRB). Alternatively, MyosinV was recruited through the MyosinV-binding domain (MBD) of melanophilin (MBD-FRB). Inducing the FKBP-Rab11 interaction with various motor proteins did not affect SEP-TfR exocytosis (Figure 3D), indicating that attachment of FKBP-Rab11 to motors does not interfere with global recycling endosome function.

First we focused on KIF1C-induced Rab11 trafficking. The addition of rapalog to neurons co-expressing KIF1C-FRB and FKBP-GFP-Rab11 induced targeting of Rab11-positive recycling endosomes from the shaft into dendritic spines (Figures S4A–S4C). Quantification in fixed neurons revealed a marked increase in the number of Rab11-targeted spines after 30 min of rapalog treatment (Figure 3E). Live-cell imaging of KIF1C-induced Rab11 vesicle dynamics within the spines showed no effect on the entry and exit speeds (Figure S4D). Interestingly, we also found an increase of non-typical spine cargoes, such as peroxisomes (Kapitein et al., 2010), into dendritic spines after KIF1C recruitment (Figures S4I–S4K). In contrast, recruitment of non-processive mutant KIF1C-T306M (Figures S4F–S4K) did not affect spine targeting. These results demonstrate that the recruitment of an active MT-based motor can result in spine entries.

We next focused on MyosinV- and VI-induced Rab11 trafficking. The addition of rapalog to neurons co-expressing MBD-FRB and FKBP-GFP-Rab11 induced a rapid burst of recycling endosomes from the shaft into many dendritic spines, but they also were able to move back out (Figures 3E–3G; Movie S3). Quantification showed that MyosinV-induced Rab11 trafficking does not increase the average entry speed (Figure 3I), but changes the number of targeted spines (Figures 3E and 3F). Interestingly, the mean exit speed was decreased by MBD recruitment, suggesting that MyosinV can oppose active spine exit events (Figure 3J). In contrast, the addition of rapalog to neurons expressing MyosinVI-FRB caused Rab11-positive recycling endosomes to move away from the spines into the dendrites (Figures 3E and 3H; Movie S4). Quantification showed that MyosinVI-induced Rab11 trafficking does not influence the average entry and exit speeds (Figures 3K and 3L). These data indicate that MyosinV- and MyosinVI-induced Rab11 trafficking primarily influence the number of targeted spines.

We next tested whether induced targeting or removal of recycling endosomes affects spine morphology. Under both conditions, we observed no differences in the total number of protrusions, spines, or filopodia 30 min after rapalog addition (Figure 4A). Cumulative frequency plots revealed that also the width and length of spines on dendrites were not changed significantly (Figure 4B). We next determined whether these manipulations influence spine growth following chemical LTP (cLTP). Consistent with previous studies (Park et al., 2004; Wang et al., 2008), cLTP stimulation using glycine treatment increased spine size in control neurons (Figure 4C). In the rapalog experiments where MBD or MyosinVI was recruited to Rab11 vesicles, the increase in spine size after cLTP was still apparent (Figure 4C). These data suggest that, under normal and cLTP conditions, induced targeting or removal of recycling endosomes does not immediately affect the morphology of dendritic protrusions.

Removal of Rab11 from Spines Decreases Surface GluA1 and PSD-95 Clusters

Given that intracellular AMPARs are transported in recycling endosomes, we explored the functional effects on synapses of induced Rab11-positive recycling endosome trafficking by measuring AMPAR-mediated miniature excitatory postsynaptic currents (mEPSCs). The influence of MyosinV-induced targeting and MyosinVI-induced removal of recycling endosomes was tested in 14- to 16-DIV neurons transfected for 3 days. During the 20-min recordings after rapalog addition, we observed no changes in the frequency or amplitude of mEPSCs among all tested conditions (Figures 4D–4F). We next analyzed surface AMPAR levels in individual spines of 20- to 22-DIV neurons by measuring SEP-GluA1 intensity before and after rapalog

(D) Induced dimerization of Rab11 vesicles with different motors does not affect fusion of TfR to the surface of COS7 cells.
(E and F) Induced dimerization of MyosinV (MBD) and KIF1C to Rab11-positive recycling endosomes increases their (E) number in dendritic protrusions, whereas coupling of MyosinV to Rab11-positive recycling endosomes removes them from spines. There is no significant effect in the (F) area of Rab11 vesicles in protrusions upon dimerization.
(G and H) (Left) Stills from time-lapse recordings of Rab11-positive recycling endosomes during which rapalog was added at time 0:00 to recruit MyosinV through (G) MBD or (H) MyosinVI. Scale bar, 5 μm. (Middle) Overlay of sequential binarized frames is color coded for time from blue to white (−10:00–0:00) and white to red (0:00–30:00); first frames are on the top. (Right) Corresponding kymographs along the length of spines show altered dynamics and localization of Rab11 vesicles upon the addition of rapalog (marked with dotted lines). Timescale is min:s.
(I–L) Quantifications of Rab11-positive recycling endosomes' (I and K) entry and (J and L) exit speeds in spines, before and after induced recruitment of (I and J) MBD or (K and L) MyosinVI, are shown.
Graphs show mean ± SEM. Statistical significance was determined using Kruskal-Wallis test and Dunn's multiple comparison post hoc test (*$p < 0.05$ and ***$p < 0.001$; A–C) and unpaired t test with Mann-Whitney correction (*$p < 0.05$, **$p < 0.01$, and ***$p < 0.001$; D–L). Scale bar, 2 μm (H). See also Figure S3 and Table S1.

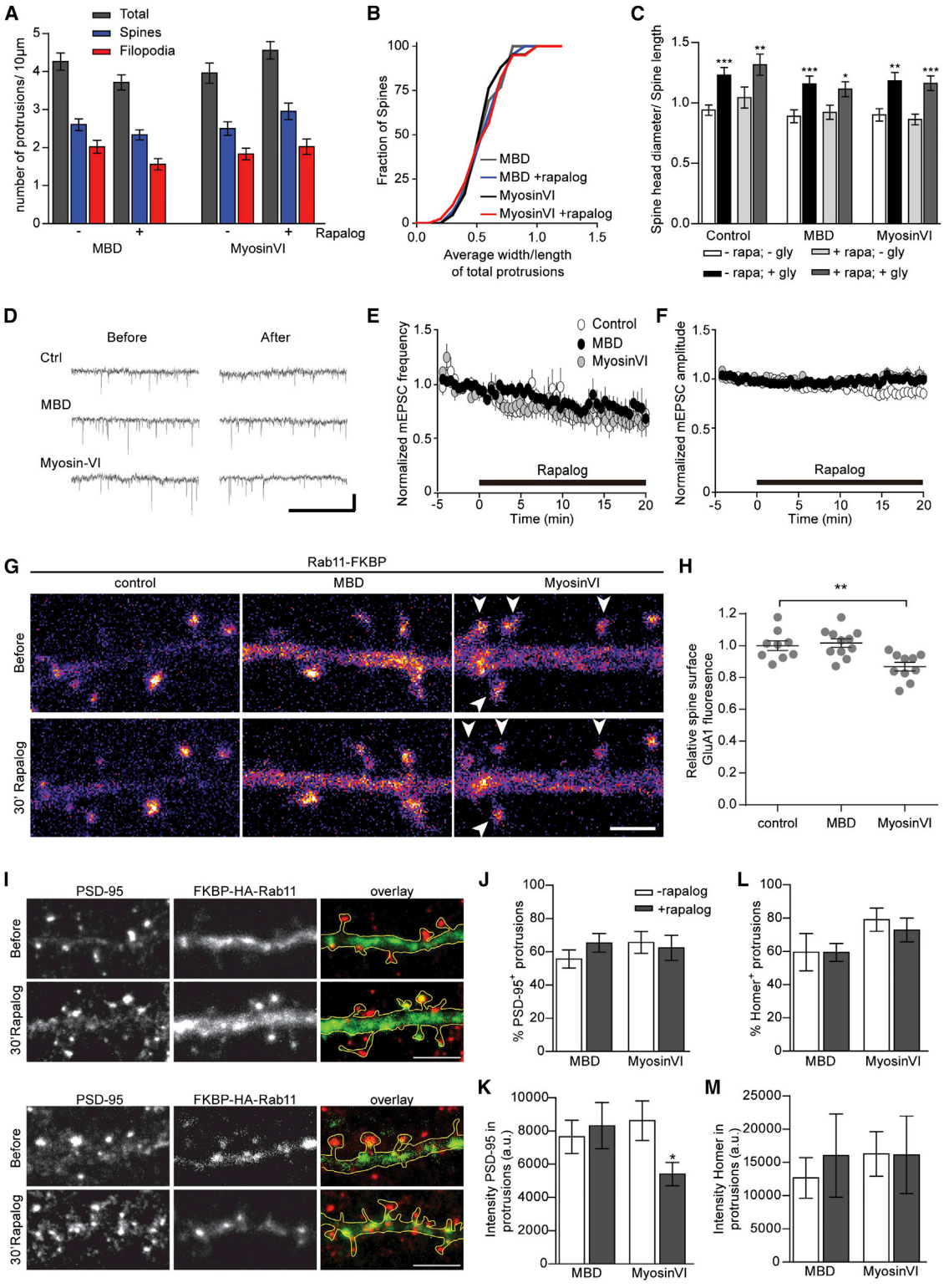

Figure 4. Removal of Recycling Endosomes Decreases Synaptic GluA1 Levels and PSD-95 Cluster Size

(A) Quantification of protrusions before and after induced dimerization of recycling endosomes to MyosinV(MBD)/VI motors is shown.

(B) Cumulative frequency of average width/length of total protrusion before and after induced dimerization of Rab11 endosomes to MBD or MyosinVI is shown.

(C) Rapalog (rapa)-induced recruitment of MBD or MyosinVI to recycling endosomes following a glycine (gly)-based cLTP protocol is shown.

(legend continued on next page)

treatment. MyosinVI-induced removal of Rab11-positive recycling endosomes from spines was associated with a marked decrease in SEP-GluA1 (Figures 4G and 4H). To determine if the short-term effects of altered Rab11-positive recycling endosome trafficking affected the structural organization of the synapse, we visualized the postsynaptic marker PSD-95 and Homer-1 clusters (Figures 4I–4M). There was a marked decrease in the intensity of PSD-95 clusters upon removal of recycling endosomes (Figures 4J and 4K), while no effect on Homer-1 was observed (Figures 4L and 4M). We conclude that removal of recycling endosomes from spines on the short-term decreases surface AMPARs and PSD-95 clusters, without affecting spine morphology and overall PSD architecture.

DISCUSSION

Here we demonstrate that AMPARs are transported in Rab11-positive recycling endosomes along MT tracks within the dendritic shaft and use both the MT and actin cytoskeleton to enter dendritic spines. Inhibiting actin or MT dynamics decreased endosome trafficking in spines. We also demonstrate that Rab11 can enter dendritic spines in a myosin (MyosinV)- and kinesin (KIF1C)-dependent manner. However, under basal conditions, the frequency of MT-spine invasions is relatively low, making actin-based transport a more generic way of driving cargo trafficking in spines. By using chemically induced dimerization to recruit MyosinV motors to Rab11-positive cargoes, we were able to control the position and trafficking of Rab11-positive recycling endosomes in spines. We demonstrate that targeting Rab11-positive recycling endosomes to spines does not significantly affect surface AMPAR levels, indicating that the supply of Rab11-positive recycling endosomes to spines is not the rate-limiting step in determining surface levels of AMPARs. On the other hand, we found that removal of Rab11-positive recycling endosomes from spines by MyosinVI was associated with a marked decrease in surface AMPAR levels and PSD-95 cluster size. We believe that this phenotype is the result of removal of the endosome from spines; however, we cannot exclude that reduced AMPAR levels are the effect of globally disrupting endosome trafficking throughout the neuron. We envision two scenarios for this effect that are not mutually exclusive. First, removal of Rab11-positive recycling endosomes could directly affect the surface expression of AMPARs by reducing the AMPAR reserve pool and decreasing endocytic recycling within spines. Second, it is possible that Rab11-positive recycling endosomes control synaptic AMPAR levels by directly or indirectly regulating PSD-95 levels at synapses. This model is interesting in light of the current observations that AMPAR density depends on structural alterations within the postsynaptic density (Bosch et al., 2014; Meyer et al., 2014).

Our results also showed that induced addition and removal of Rab11 recycling endosomes from spines for short time periods does not have an impact on spine growth following cLTP stimulation. This is an interesting finding because it shows that local translocation of Rab11 vesicles for a short time interval (~30-min rapalog treatment), is not sufficient to cause the plasticity changes that were observed previously after longer-term blockage of endosomal recycling (Park et al., 2004; Wang et al., 2008). Future work will be needed to resolve the precise chronology of the various trafficking events during LTP and to determine which specific organelles and spine substructures are remodeled over different time periods. Based on the involvement of endosomes in mediating signal transduction responses in other systems (Miaczynska et al., 2004), our findings imply that the specific positioning of recycling endosomes is an important factor in controlling different aspect of synapse architecture.

EXPERIMENTAL PROCEDURES

Expression Constructs

Fluorescently or HA-tagged MyosinVI(1-1041)-FRB, MBD(147-240)-FRB, and PEX-FKBP heterodimerization constructs have been described previously (Kapitein et al., 2010). All other constructs were created using PCR-based strategies. Fluorescently or HA-tagged FKBP-Rab11, KIF1C(1-496)-FRB, and KIF1C(1-496)-T306M-FRB (rigor mutant) were generated in GW1 and/or pβ-actin expression vectors. For details see the Supplemental Experimental Procedures.

Hippocampal Neuron Cultures, Transfections, and Electrophysiology

Primary hippocampal cultures were prepared from embryonic day 18 (E18) rat brains (Jaworski et al., 2009). For electrophysiology experiments, hippocampal primary cultures were prepared from post-natal day 1–3 C57BL6 mice of either sex, as described previously (Hoogenraad et al., 2010). For details see the Supplemental Experimental Procedures.

Live-Cell Imaging Microscopy

Live-cell imaging was performed using two-color total internal reflection fluorescence (TIRF) or laser confocal spinning-disk microscopy. All imaging was performed in full conditioned Neurobasal medium at 37°C and 5% CO_2 unless

(D–F) Sample traces of mEPSCs recorded before and 20 min after the application of rapalog (scale bar, 20 pA/2 s). Summary graph shows the averaged time course of (E) frequency and (F) amplitude of mEPSCs. Averaged mEPSC amplitudes and frequencies were measured every 30 s, and the values were normalized to the values measured during the baseline period (−5 to 0 min). Rapalog (100 nM) was applied at 0 min.

(G) Typical examples of SEP-GluA1 levels in dendrites expressing Rab11-FKBP and mCherry (control), mRFP-MBD-FRB, or MyosinVI-mRFP-FRB before and after 30 min of rapalog addition. Images are pseudocolored for intensity (purple, low; and yellow/white, high).

(H) Quantification of relative average SEP-GluA1 fluorescence intensity after 30 min rapalog treatment in dendritic spines of neurons expressing mCherry (control), mRFP-MBD-FRB, or MyosinVI-mRFP-FRB is shown.

(I) Immunostaining of dendritic protrusions with PSD-95 (red) before and after induced dimerization of Rab11 recycling endosomes (green) to MBD or MyosinVI is shown.

(J and K) Quantifications of number of (J) PSD-95-positive protrusions and (K) PSD-95 intensity per 10-μm regions of dendrite, before and after induced dimerization of Rab11 endosomes to MBD or MyosinVI, are shown.

(L and M) Quantifications of number of Homer-positive protrusions (L) and Homer intensity (M) per 10 μm dendritic region, before and after induced dimerization of Rab11 to MBD or Myosin VI, are shown.

Graphs show mean ± SEM. Statistical significance was determined using an unpaired t test with Mann-Whitney correction (*$p < 0.05$, **$p < 0.01$, and ***$p < 0.001$; C and J–M) and one-way ANOVA and Bonferroni multiple comparison post hoc test (**$p < 0.01$; H). Scale bar, 2 μm (G) and 5 μm (I). See also Table S1.

otherwise indicated. For details see the Supplemental Experimental Procedures.

Live-Cell Imaging of Rab11 and GFP-GluA2 Dynamics

To probe intracellular AMPA receptor vesicle transport in neurons, we co-expressed pTRE-GFP-GluA2 with HA-GluA1 and precisely controlled the timing and level of GluA2 expression using a DOX-regulated gene expression system. To image Rab11-positive recycling endosome dynamics in dendritic spines, time lapses of 5 min were acquired, with a 5-s interval between acquisitions. For details see the Supplemental Experimental Procedures.

Live-Cell Imaging and Analysis of Rab11 and SEP-GluA1 Dynamics

To visualize exocytic events of Rab11-positive recycling endosomes containing AMPA receptors, we performed simultaneous dual-color imaging of tagRFP-Rab11 and SEP-GluA1 at 2 frames/s for up to 3 min. Events showing sudden local increases of SEP fluorescence were manually counted in ImageJ and classified as spine or dendritic events. To quantify the membrane-bound amount of GluA1 in rapalog experiments, background-subtracted maximum projections of SEP-GluA1 fluorescence intensity before and after 30 min of rapalog treatment in ~15 randomly selected spines per imaged dendrite were measured in ImageJ and expressed as ratios. These ratios were then averaged per dendrite. For details see the Supplemental Experimental Procedures.

Statistical Methods

Unless otherwise noted, the graphs represent mean ± SEM. Statistical significance was determined using the Kruskal-Wallis test or one-way ANOVA and Dunn's multiple comparison post hoc test, Wilcoxon test for paired data, and an unpaired t test with Mann-Whitney correction (* $p < 0.05$, ** $p < 0.01$, and *** $p < 0.001$). The statistical test(s) used for each experiment is indicated in each figure legend. The exact value of n (number of neurons analyzed) and N (number of independent experiments) and the mean ± SEM for each graph presented in the paper are summarized in Table S1.

SUPPLEMENTAL INFORMATION

Supplemental Information includes Supplemental Experimental Procedures, four figures, one table, and four movies and can be found with this article online at http://dx.doi.org/10.1016/j.celrep.2015.09.062.

AUTHOR CONTRIBUTIONS

M.E.d.S., M.A., P.S., J.L., and L.C.K. performed experiments. M.E.d.S., M.A., and L.C.K. analyzed the data. T.W., S.C., and K.F. performed electrophysiology experiments and analyzed the data. M.E.d.S., L.C.K., and C.C.H. designed the research and wrote the paper. C.J.W., L.C.K., and C.C.H. supervised the project.

ACKNOWLEDGMENTS

We are grateful to Dr. Terunaga Nakagawa for pTRE-GFP-GluA1-FLAG, Dr. Daniel Choquet for SEP-GluA1, and Dr. Folma Buss for Myosin VI tail construct. This work was supported by the Erasmus Medical Center (EMC fellowship to L.C.K.), the Netherlands Organization for Scientific Research (NWO-ALW-VENI to L.C.K. and NWO-ALW-VICI to C.C.H.), the Netherlands Organization for Health Research and Development (ZonMW-TOP to C.C.H. and ZonMW-VIDI to C.J.W.), and EMBO Young Investigators Program ([YIP] to C.C.H.). This work is part of the research programme of the Foundation for Fundamental Research on Matter (FOM), which is part of the Netherlands Organization for Scientific Research. M.E.d.S. is supported by Fundação para a Ciência e Tecnologia (FCT-Portugal). P.S. is supported by the Swiss National Science Foundation (SNSF). J.L. is supported by International Ph.D. Project Programme of Foundation for Polish Science (studies of nucleic acids and proteins-from basic to applied research) cofinanced by the European Union-Regional Development Fund and cosupervised by professor Jacek Jaworski. K.F. was supported by the Whitehall Foundation (2012-08-44) and Japan Foundation for Pediatric Research (JFPR).

Received: June 10, 2014
Revised: August 20, 2015
Accepted: September 21, 2015
Published: October 22, 2015

REFERENCES

Adrian, M., Kusters, R., Wierenga, C.J., Storm, C., Hoogenraad, C.C., and Kapitein, L.C. (2014). Barriers in the brain: resolving dendritic spine morphology and compartmentalization. Front. Neuroanat. *8*, 142.

Bosch, M., Castro, J., Saneyoshi, T., Matsuno, H., Sur, M., and Hayashi, Y. (2014). Structural and molecular remodeling of dendritic spine substructures during long-term potentiation. Neuron *82*, 444–459.

Brown, T.C., Correia, S.S., Petrok, C.N., and Esteban, J.A. (2007). Functional compartmentalization of endosomal trafficking for the synaptic delivery of AMPA receptors during long-term potentiation. J. Neurosci. *27*, 13311–13315.

Colgan, L.A., and Yasuda, R. (2014). Plasticity of dendritic spines: subcompartmentalization of signaling. Annu. Rev. Physiol. *76*, 365–385.

Correia, S.S., Bassani, S., Brown, T.C., Lisé, M.F., Backos, D.S., El-Husseini, A., Passafaro, M., and Esteban, J.A. (2008). Motor protein-dependent transport of AMPA receptors into spines during long-term potentiation. Nat. Neurosci. *11*, 457–466.

Czöndör, K., Mondin, M., Garcia, M., Heine, M., Frischknecht, R., Choquet, D., Sibarita, J.B., and Thoumine, O.R. (2012). Unified quantitative model of AMPA receptor trafficking at synapses. Proc. Natl. Acad. Sci. USA *109*, 3522–3527.

Gu, J., Firestein, B.L., and Zheng, J.Q. (2008). Microtubules in dendritic spine development. J. Neurosci. *28*, 12120–12124.

Hoogenraad, C.C., Popa, I., Futai, K., Martinez-Sanchez, E., Wulf, P.S., van Vlijmen, T., Dortland, B.R., Oorschot, V., Govers, R., Monti, M., et al. (2010). Neuron specific Rab4 effector GRASP-1 coordinates membrane specialization and maturation of recycling endosomes. PLoS Biol. *8*, e1000283.

Hu, X., Viesselmann, C., Nam, S., Merriam, E., and Dent, E.W. (2008). Activity-dependent dynamic microtubule invasion of dendritic spines. J. Neurosci. *28*, 13094–13105.

Huganir, R.L., and Nicoll, R.A. (2013). AMPARs and synaptic plasticity: the last 25 years. Neuron *80*, 704–717.

Jaworski, J., Kapitein, L.C., Gouveia, S.M., Dortland, B.R., Wulf, P.S., Grigoriev, I., Camera, P., Spangler, S.A., Di Stefano, P., Demmers, J., et al. (2009). Dynamic microtubules regulate dendritic spine morphology and synaptic plasticity. Neuron *61*, 85–100.

Kapitein, L.C., Schlager, M.A., van der Zwan, W.A., Wulf, P.S., Keijzer, N., and Hoogenraad, C.C. (2010). Probing intracellular motor protein activity using an inducible cargo trafficking assay. Biophys. J. *99*, 2143–2152.

Kapitein, L.C., van Bergeijk, P., Lipka, J., Keijzer, N., Wulf, P.S., Katrukha, E.A., Akhmanova, A., and Hoogenraad, C.C. (2013). Myosin-V opposes microtubule-based cargo transport and drives directional motility on cortical actin. Curr. Biol. *23*, 828–834.

Meyer, D., Bonhoeffer, T., and Scheuss, V. (2014). Balance and stability of synaptic structures during synaptic plasticity. Neuron *82*, 430–443.

Miaczynska, M., Pelkmans, L., and Zerial, M. (2004). Not just a sink: endosomes in control of signal transduction. Curr. Opin. Cell Biol. *16*, 400–406.

Nash, J.E., Appleby, V.J., Corrêa, S.A., Wu, H., Fitzjohn, S.M., Garner, C.C., Collingridge, G.L., and Molnár, E. (2010). Disruption of the interaction between myosin VI and SAP97 is associated with a reduction in the number of AMPARs at hippocampal synapses. J. Neurochem. *112*, 677–690.

Newpher, T.M., and Ehlers, M.D. (2008). Glutamate receptor dynamics in dendritic microdomains. Neuron *58*, 472–497.

Osterweil, E., Wells, D.G., and Mooseker, M.S. (2005). A role for myosin VI in postsynaptic structure and glutamate receptor endocytosis. J. Cell Biol. *168*, 329–338.

Park, M., Penick, E.C., Edwards, J.G., Kauer, J.A., and Ehlers, M.D. (2004). Recycling endosomes supply AMPA receptors for LTP. Science *305*, 1972–1975.

Park, M., Salgado, J.M., Ostroff, L., Helton, T.D., Robinson, C.G., Harris, K.M., and Ehlers, M.D. (2006). Plasticity-induced growth of dendritic spines by exocytic trafficking from recycling endosomes. Neuron *52*, 817–830.

Petrini, E.M., Lu, J., Cognet, L., Lounis, B., Ehlers, M.D., and Choquet, D. (2009). Endocytic trafficking and recycling maintain a pool of mobile surface AMPA receptors required for synaptic potentiation. Neuron *63*, 92–105.

Wagner, W., Brenowitz, S.D., and Hammer, J.A., 3rd. (2011). Myosin-Va transports the endoplasmic reticulum into the dendritic spines of Purkinje neurons. Nat. Cell Biol. *13*, 40–48.

Wang, Z., Edwards, J.G., Riley, N., Provance, D.W., Jr., Karcher, R., Li, X.D., Davison, I.G., Ikebe, M., Mercer, J.A., Kauer, J.A., and Ehlers, M.D. (2008). Myosin Vb mobilizes recycling endosomes and AMPA receptors for postsynaptic plasticity. Cell *135*, 535–548.

Yau, K.W., van Beuningen, S.F., Cunha-Ferreira, I., Cloin, B.M., van Battum, E.Y., Will, L., Schätzle, P., Tas, R.P., van Krugten, J., Katrukha, E.A., et al. (2014). Microtubule minus-end binding protein CAMSAP2 controls axon specification and dendrite development. Neuron *82*, 1058–1073.